The distribution of solar wind speeds during solar minimum: calibration for numerical solar wind modeling constraints on the source of the slow solar wind

The distribution of solar wind speeds during solar minimum: Calibration for numerical solar wind modeling constraints on the source of the slow solar wind

S. L. McGregor,[1] W. J. Hughes,[1] C. N. Arge,[2] M. J. Owens,[3] and D. Odstrcil[4]

Received 30 June 2010; revised 1 November 2010; accepted 7 December 2010; published 1 March 2011.

[1] It took the solar polar passage of Ulysses in the early 1990s to establish the global structure of the solar wind speed during solar minimum. However, it remains unclear if the solar wind is composed of two distinct populations of solar wind from different sources (e.g., closed loops which open up to produce the slow solar wind) or if the fast and slow solar wind rely on the superradial expansion of the magnetic field to account for the observed solar wind speed variation. We investigate the solar wind in the inner corona using the Wang-Sheeley-Arge (WSA) coronal model incorporating a new empirical magnetic topology–velocity relationship calibrated for use at 0.1 AU. In this study the empirical solar wind speed relationship was determined by using Helios perihelion observations, along with results from Riley et al. (2003) and Schwadron et al. (2005) as constraints. The new relationship was tested by using it to drive the ENLIL 3-D MHD solar wind model and obtain solar wind parameters at Earth (1.0 AU) and Ulysses (1.4 AU). The improvements in speed, its variability, and the occurrence of high-speed enhancements provide confidence that the new velocity relationship better determines the solar wind speed in the outer corona (0.1 AU). An analysis of this improved velocity field within the WSA model suggests the existence of two distinct mechanisms of the solar wind generation, one for fast and one for slow solar wind, implying that a combination of present theories may be necessary to explain solar wind observations.

Citation: McGregor, S. L., W. J. Hughes, C. N. Arge, M. J. Owens, and D. Odstrcil (2011), The distribution of solar wind speeds during solar minimum: Calibration for numerical solar wind modeling constraints on the source of the slow solar wind, *J. Geophys. Res.*, *116*, A03101, doi:10.1029/2010JA015881.

1. Introduction

[2] During a archetypical sunspot minimum few if any active regions litter the solar surface, coronal holes are confined primarily to the Sun's poles, and white light images show a simple near-equatorial helmet streamer structure. *In situ* solar wind observations made near the ecliptic plane reveal a slow and variable solar wind punctuated by occasional fast solar wind streams. The fast streams are traditionally associated with coronal hole sources but there is less consensus on the source of the slow solar wind. Some argue that the slow solar wind can be explained by wave acceleration processes governed by the coronal magnetic configuration (e.g., *Wang and Sheeley* [1990] or *Cranmer et al.* [2007]), while others argue that the slow solar wind is produced by an inherently dynamic process [e.g., *Fisk et al.*, 1998; *Schwadron and McComas*, 2003], and that the solar wind speed/magnetic field expansion relationship is coincidental and is merely a result of the coronal geometry.

[3] *Wang and Sheeley* [1990] found an empirical correlation between the geometry of the coronal magnetic field and solar wind speed. Specifically they found that the amount a magnetic flux tube expands between the photosphere and a source surface placed at 2.5 solar radii is inversely related to the solar wind speed, with large, superradial magnetic expansions producing slow solar wind. *Cranmer* [2005] explained the physical basis of this relationship in terms of the expansion of the magnetic field being tied to the location of the critical point in the corona. Magnetic flux tubes that have large expansion factors have critical points located further away from the photosphere than those with small expansion factors. Assuming the corona is heated by incompressible Alfven waves that are partially reflected and damped via a turbulent cascade, the rate of the expansion of the magnetic field determines whether the waves are reflected and damped above or below the critical point. On flux tubes with large expansion factors the heating occurs in the subsonic corona below the critical point, resulting in an increased scale height and mass flux, while keeping the kinetic energy of the flow fairly constant, whereas on flux

[1]Astronomy Department, Boston University, Boston, Massachusetts, USA.
[2]Kirtland Air Force Base, Albuquerque, New Mexico, USA.
[3]Department of Meteorology, University of Reading, Reading, UK.
[4]NASA Goddard Space Flight Center, Greenbelt, Maryland, USA.

0148-0227/11/2010JA015881

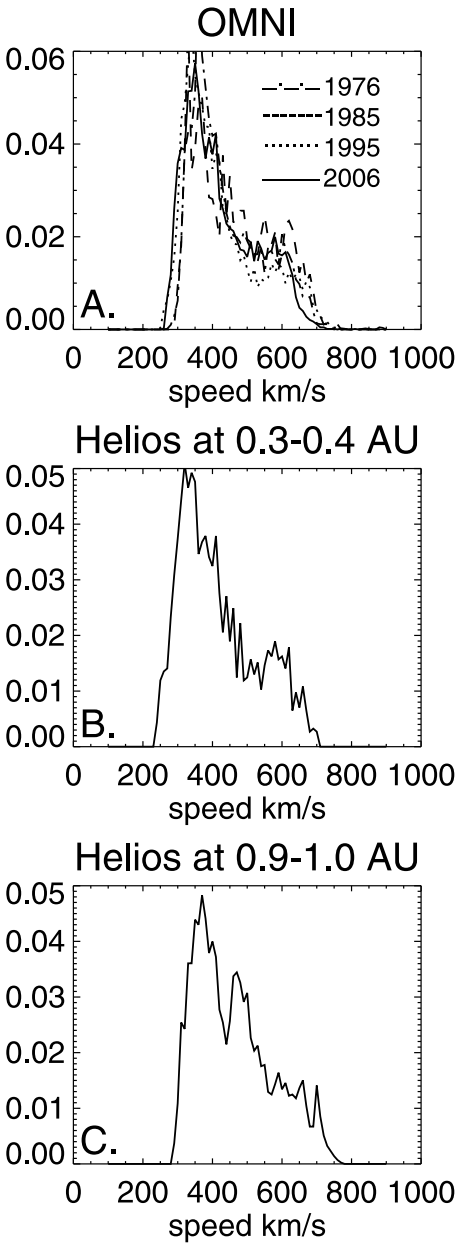

Figure 1. Normalized solar wind speed distributions during solar minimum. (a) OMNI solar wind observations during the solar minimum years 2006 (solid), 1995 (dotted), 1985 (dashed), and 1976 (dash-dotted). (b) The distribution observed by Helios between 0.3 and 0.4 AU. (c) The distribution observed by Helios between 0.9 and 1.0 AU.

tubes with small expansion factors the heating occurs in the supersonic corona, where the energy goes into the kinetic energy of the solar wind, increasing the flow speed [*Leer and Holzer*, 1980; *Pneuman*, 1980]. Using this model and a simplified coronal magnetic field configuration [*Banaszkiewicz et al.*, 1998], *Cranmer et al.* [2007] obtained solar wind speeds equivalent to those observed by the Ulysses fast latitude scan in 1995. *Wang et al.* [2009] also argue that similar processes control the high- and low-speed wind. They conclude that at least some of the observed compositional differences between the fast and slow solar wind can be attributed to variations in expansion factor and foot point magnetic field strength and therefore it is unnecessary to invoke a source on closed field lines for the bulk of the low-speed solar wind.

[4] In contrast to these quasi steady state ideas, *Fisk et al.* [1998] argue that the source of the solar wind is inherently dynamic, with magnetic fields constantly reconfiguring due to foot point motions and undergoing interchange reconnection as they meander their way through coronal holes and across the solar surface. As closed loops open, the plasma on them escapes to form the solar wind. The fast solar wind, with cooler ionization temperatures, comes from either small loops that continually reconnect with open flux tubes or from more permanently open flux tubes in coronal holes, while slow solar wind, with higher ionization temperatures, comes from larger and hotter loops that intermittently reconnect with open flux tubes surrounding coronal holes [*Schwadron and McComas*, 2003; *Fisk and Schwadron*, 2001]. If the coronal field is approximated as a potential field, solar wind speed will be independent of the radial or superradial expansion [*Fisk et al.*, 2003]. They argue that correlation between expansion factor and solar wind speed coincidentally results from the geometry of the coronal magnetic field.

[5] The question arises, are the fast and slow solar wind merely two extremes of the same process or is the solar wind composed of different populations with different acceleration mechanisms? The work we describe in this paper arose from an attempt to better calibrate the empirical velocity relationship used in the Wang-Sheeley-Arge (WSA) model at 0.1 AU which is then propagated out into the heliosphere using the ENLIL solar wind model. ENLIL is a 3-D Magnetohydrodynamic (MHD) model of the heliosphere [*Odstrcil*, 2003] requiring a coronal model on its inner boundary at 0.1 AU. Traditionally WSA has been used in conjunction with a ballistic propagation model to empirically predict solar wind velocities at 1.0 AU. However, to provide an inner boundary condition for ENLIL, WSA must provide a realistic solar wind speed in the outer corona (0.1 AU) instead. *Owens et al.* [2008] showed this requires a new calibration of the WSA velocity equation. To better calibrate the WSA velocity equation we first compare the distributions of solar wind speeds observed around solar minimum near Earth and by Helios, which obtained solar wind observations in the inner (<1.0 AU) heliosphere. In section 3 we describe the models and in section 4 we use observations made by Helios and others to recalibrate the WSA empirical velocity relationship to give velocities at 0.1 AU. We test this new formula in section 5 by comparing WSA-ENLIL predictions with observations made near Earth and by Ulysses during the 1995 fast latitude scan. Having validated the new formula we then discuss its ramifications and what it can tell us about the sources of the fast and slow solar wind.

2. Observed Solar Wind Speed Distributions

[6] Figure 1 compares solar wind speed distributions observed near Earth with those obtained in the inner heliosphere. Figure 1a shows the normalized occurrence distributions of solar wind speeds observed near Earth obtained from the OMNI data set. Each curve is constructed from 1 year's data obtained during each of the past four solar

minima. The solid, dashed, dotted and dash-dotted lines show observations from 2006, 1995, 1985, and 1976, respectively. During these years almost all observations are confined between 240 km/s and 750 km/s and show a bimodal distribution, with a large slow solar wind component with a peak at about 350 km/s, and a smaller fast solar wind component with a peak around 600 km/s. Since this work focuses on solar minimum when the heliospheric current sheet tends to be flatter and lie closer to the ecliptic plane, a greater fraction of slow solar wind than fast solar wind is expected to be observed. More importantly, the distributions are bimodal rather than smoothly varying, suggesting two distinct types of solar wind. Helios had a highly elliptical orbit in the ecliptic plane and obtained the solar wind observations made closest to the Sun to date. Figure 1b shows the normalized solar wind speed occurrence distributions observed by Helios in 1974–1976 during four perihelion passes when it was between 0.3 and 0.4 AU, while Figure 1c shows the distribution observed during three full and two partial aphelion passes when Helios was between 0.9 and 1.0 AU. We used a 3 year interval centered about solar minimum to increase the number of individual observations and hence improve the statistics. The distribution observed near aphelion (Figure 1c) is similar to those obtained from the OMNI data set in Figure 1a. Both distributions are bimodal with the main peak between 350–400 km/s and a secondary fast wind plateau around 650 km/s. There are very few observations less than 300 km/s or greater than 750 km/s. In contrast, the distribution observed near perihelion (Figure 1b) has a slightly more pronounced bimodal structure. The slow solar wind peak is between 300 and 350 km/s, slower than at 1 AU, while the fast wind has a distinct separate peak around 600 km/s. The solar wind closer to the Sun is expected to have higher-velocity shears and more abrupt jumps in the solar wind speeds than is seen further out in the heliosphere [*Gosling et al.*, 1978], consistent with the clearer bimodal structure seen in Figure 1b.

3. WSA-ENLIL Model

[7] The Wang Sheeley Arge (WSA) model is a combination of a Potential Field Source Surface (PFSS) model and a Schatten Current Sheet (SCS) model [*Arge and Pizzo*, 2000; *Arge et al.*, 2003, 2004; *McGregor et al.*, 2008] which uses synoptic maps of line-of-sight (LOS) observations of the Sun's photospheric magnetic field as input. The synoptic maps, mapped onto a 2.5 degree resolution grid, define the inner boundary to the PFSS model [*Schatten et al.*, 1969; *Altschuler and Newkirk*, 1969], that determines the coronal field out to 2.5 solar radii. The radial field at the 2.5 solar radii surface is used as input into the SCS model [*Schatten*, 1971], which assumes no volumetric currents save at the polarity inversion, and provides a more realistic magnetic field topology for the upper corona.

[8] *Arge et al.* [2003, 2004] developed an empirical formula [*Arge et al.*, 2004, equation (1)] that gives the solar wind speed at 1.0 AU as a function of two parameters derived from the coronal magnetic field, the flux tube expansion factor (given by equation (1)), normalized such that $f_s = 1$ for purely radial expansion, and the minimum angular separation (at the photosphere) between an open magnetic field line footprint and its nearest open flux boundary (θ_b). Their relationship effectively combined the Wang-Sheeley model [*Wang and Sheeley*, 1990, 1992] who based solar wind velocity solely on the value of f_s and the model of *Riley et al.* [2001] who based the solar wind speed solely on the value of θ_b.

$$f_s = \frac{B(1R_\odot)}{2.5^2 B(2.5R_\odot)} \tag{1}$$

Arge et al.'s empirical formula was calibrated by propagating the speeds to Earth using a one-dimensional modified kinematic code [*Arge and Pizzo*, 2000] and comparing to observations there. The values of constants within the equation were varied until comparisons with 1 AU observations yielded qualitatively good results. Thus the solar wind distributions obtained from WSA give a good representation of the velocities observed at 1AU when used in conjunction with a 1-D kinematic propagation model. The WSA model yields good results in both comparisons with coronal hole boundaries [*de Toma et al.*, 2005; *de Toma and Arge*, 2005] and with solar wind speed observations at 1 AU [*Arge et al.*, 2004; *Owens et al.*, 2008]. Since the empirical velocity relationship was derived using observations at 1 AU and a kinematic propagation model that does not contain any solar wind acceleration nor all the physics of stream interactions, it cannot be expected to give reliable velocities at 0.1 AU.

[9] ENLIL is a 3-D MHD heliospheric code that uses a polytropic energy equation with $\gamma = 1.5$ [*Odstrcil*, 2003]. The inner boundary of ENLIL is at 0.1 AU (21.5 $R_\odot$), well beyond the point where the solar wind becomes supersonic and super-Alfvenic. In this paper the inner boundary conditions, specifically the structure of the radial magnetic field and the solar wind velocity at this boundary, are provided by WSA. As ENLIL is a full 3-D MHD model, the solar wind continues to accelerate within its volume and stream interactions cause both accelerations and decelerations of the flow. Since this physics is not included in the kinematic propagation model used to calibrate the WSA velocity formula, using the unmodified WSA velocity formula to provide input to ENLIL will give solar winds that are generally too fast at Earth.

[10] *Owens et al.* [2008] systematically compared the "original" version of the WSA-ENLIL model (and two other models) with 8 years of L1 observations. The *Owens et al.* [2008] version uses an ad hoc modification of the WSA velocity formula to provide the velocity at the inner boundary of ENLIL. This velocity is obtained by taking the velocity given by *Owens et al.* [2008, equation (3)], subtracting 50 km/s to account for the acceleration within ENLIL, and limiting the range of speeds to between 275 and 625 km/s. If the speed is outside this range it is raised to 275 km/s or lowered to 625 km/s as appropriate. At the ENLIL inner boundary the azimuthal and meridional components of the velocity are set to zero, the plasma number density is chosen to ensure a uniform momentum flux (nv^2), and the plasma temperature is set to ensure uniform plasma pressure (nkT). The polarity of the magnetic field is taken from WSA, but the magnitude and direction are recomputed. The radial component of the magnetic field has the sign provided by WSA and a magnitude proportional to the radial velocity such that in the highest-speed wind (625 km/s) the radial magnetic field component is 300 nT. The azimuthal magnetic field com-

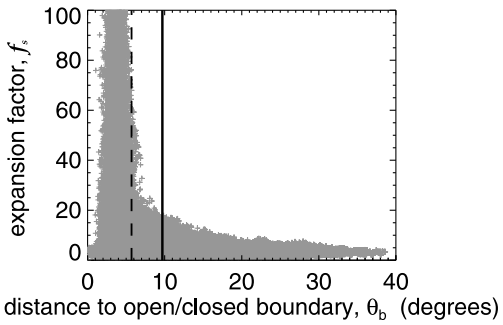

Figure 2. Scatterplot of the expansion factor versus distance from the open flux boundary of all open flux tubes in the WSA model for 41 Carrington rotations (1890–1930) during solar minimum. The vertical lines are at open flux region boundaries of ~6° and ~10°.

ponent is given by the Parker spiral angle while the meridional component is set to zero.

[11] *Owens et al.* [2008] found that the original WSA-ENLIL model matched the observed mean solar wind speeds very well over the solar cycle, but that the variability and range of the predicted solar wind was much lower than observed, speeds were too high within slow streams and too low in fast streams. Furthermore the transitions between slow and fast streams were broad, instead of the observed sharp boundary. These results suggest that the velocities calculated at 0.1 AU using the original empirical formula do not accurately reflect the coronal velocity distribution at 0.1 AU.

[12] In section 4 we attempt to improve the empirical velocity relationship. We use studies by *Riley et al.* [2003] and *Schwadron et al.* [2005], in conjunction with Helios perihelion observations to better estimate four of the parameters in the original solar wind speed relationship so that the relationship can be used directly as an ENLIL boundary condition without using the ad hoc modifications described earlier. In section 5 we use the new velocity relationship in WSA-ENLIL and compare the results with those obtained using the original relationship and with observations. We find that the new velocity relationship gives better predictions.

4. Recalibrating the WSA Velocity Relationship

[13] In order to adapt the WSA for use with ENLIL, we begin by taking the empirical velocity relationship in the form

$$V(f_s,\theta_b) = V_o + \left(\frac{V_1}{(1+f_s)^{\frac{2}{9}}}\right) * \left(\left(1.0 - 0.8\exp\left(-\left(\frac{\theta_b}{\phi}\right)^{\beta}\right)\right)^3\right) \quad (2)$$

which is very similar in form to *Arge et al.* [2004, equation (1)] and *Owens et al.* [2008, equation (3)], but the parameterization is in the form of more observable quantities and has constants which are consistent with the current version of WSA (using NSO magnetograms), in operation at the Space Weather Prediction Center (SWPC at http://www.swpc.noaa.gov/ws/). Four parameters remain to be determined, V_o, V_1, ϕ, and β, which have values of 240, 675, 2.8, and 1.25, respectively, in the WSA version at SWPC. Both V_o and V_1 have units of velocity: V_o sets the minimum possible solar wind speed while V_1 determines the maximum speed. The angle ϕ and exponent β determine the angular extent and influence of the open flux boundary layer, respectively. For a simple calibration of the velocity relationship, any of the parameters within equation (2) could have been modified. However, the parameters V_o, V_1, ϕ, and β, were found to vary in such a way as to be constrained by the Helios measurements and work by *Riley et al.* [2003] and *Schwadron et al.* [2005].

[14] Before proceeding it is worth examining the ranges of the parameters f_s and θ_b obtained from the WSA magnetic fields. Figure 2 shows the distribution of f_s and θ_b for all open flux tubes obtained from the WSA model for 41 Carrington rotations (1891–1931) that span the solar minimum years 1995–1997. This distribution is clearly far from uniform. Large expansion factors ($f_s > 20$) only occur on flux tubes whose photospheric magnetic foot points lie close ($\theta_b < 7°$) to an open/closed flux boundary. Flux tubes whose foot points are far from an open/closed flux boundary ($\theta_b > 20°$) have relatively small superradial expansion factors ($f_s < 10$). The values of f_s and θ_b are strongly correlated, so it is not surprising that both parameters can do a reasonable job of predicting solar wind speed by themselves, at least near solar minimum. However, the correlation is not perfect, so a combination of both parameters should, in principle, be able to predict velocity better than either parameter alone, assuming that is, that both parameters do affect solar wind speed.

[15] The functional form of equation (2) is illustrated in Figure 3 which shows solar wind speed as a function of θ_b for various values of f_s. The line color indicates the value of f_s which varies from 1 (red) to 99 (blue) in increments of 2. The general shape of the curves shows the effect of both parameters, θ_b and f_s. When flux tubes originate very close to the edge of an open flux region (θ_b small) the solar

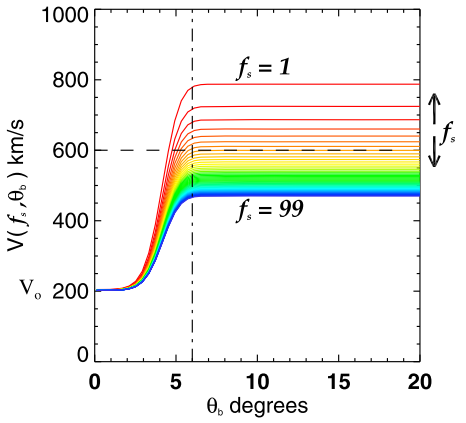

Figure 3. Graphical representation of the WSA empirical solar wind speed relationship (equation (1)) using the parameter values determined in this paper. Solar wind speed is plotted as a function of distance from the open flux boundary (θ_b) for different values of the expansion factor (f_s) indicated by color ranging from 1 (red) to 99 (blue) in increments of 2. The vertical line is at $\theta_b \approx 6°$, and the dashed line is at V_{SW} = 600 km/s.

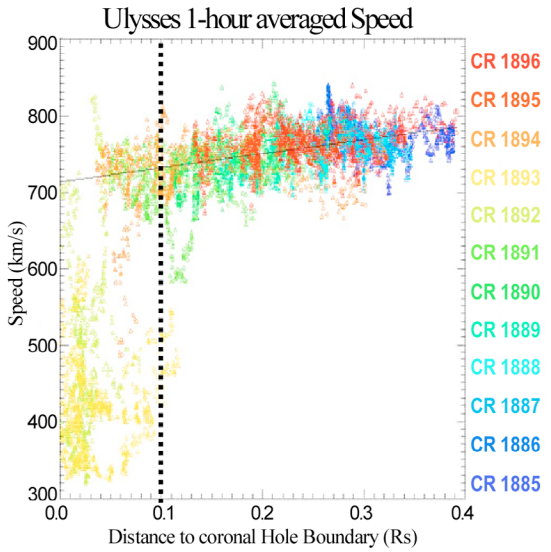

Figure 4. Solar wind speed versus distance to the open flux boundary for 12 Carrington rotations during the first Ulysses fast latitude scan wind [from *Riley et al.*, 2003]. The dotted vertical line at 0.1 $R_\odot$ (5.7°) divides most of the slow solar wind from the faster.

wind speed is close to the minimum speed, V_0, irrespective of the value of f_s. For flux tubes whose foot points are well away from the open/closed flux boundary (θ_b large), the speed reaches an asymptotic value that depends only on f_s. Between these two extremes the speed monotonically increases with θ_b over a boundary layer several degrees wide. The parameters ϕ and β in equation (1) control the width and location of this boundary layer. The value of ϕ determines the value of θ_b at which the speed begins to increase while β determines the value of θ_b at which the speed approaches its asymptotic value.

[16] Observations made as close as possible to the 0.1 AU inner boundary of ENLIL would be best for calibrating the velocity relationship. The closest observations that have been made are those made by Helios which had an elliptical orbit in the ecliptic plane with perihelion near 0.3 AU. Though Helios orbited the Sun between 1974 and 1981, we confine the observations to those made during solar minimum (1974–1976), to be consistent as possible with the other solar minimum observations used in this study. Helios observed solar wind speeds as low as 200 km/s and maximum speeds near 800 km/s (Figure 1b). Our recalibrated velocity relationship must produce speeds which encompass this range as well as have a distribution of velocities similar to that observed by Helios.

[17] Figure 4 is taken from *Riley et al.* [2003] who took Ulysses solar wind observations made at solar minimum, mapped them ballistically from Ulysses to the outer boundary of a coronal MHD model at 30 $R_\odot$, then used the model to magnetically map to the source regions on the solar surface. The solar wind speed is plotted versus the distance of the source region from the closest open/closed flux boundary in solar radii, equivalent to angular distance in radians. The different colors indicated observations from twelve different Carrington rotations. Note that *Riley et al.* [2003] found that all slow solar wind (V_{SW} < 600 km/s) comes from regions close to the open/closed boundary. The dotted black vertical line indicates the distance beyond which almost no slow solar wind (below 600 km/s) occurs. This distance is equivalent to little less than 6°, which can used to further constrain the velocity relationship.

[18] Our final observational constraint is provided by *Schwadron et al.* [2005] who found that during solar minimum the solar wind with intermediate speeds (600–740 km/s) comes from a coronal hole boundary layer about 4° wide on the photosphere. Within this layer, freezing in temperatures and speed vary monotonically and are anticorrelated. They suggest that as the source region is located further away from the open flux boundary, a decrease in the expansion factor, and therefore flow speed, could cause ions to freeze in at a lower height and hence cooler temperature. We use this 4° wide layer to further constrain the expansion factor term in the velocity relationship.

4.1. Inner Heliosphere Solar Wind Velocity Distributions

[19] Figure 1b shows the distribution of solar wind speeds observed by Helios near its perihelion. Since these are the only solar wind measurements available from the inner heliosphere they provide the best observations to compare with speeds obtained from the WSA empirical relationship. The Kitt Peak National Solar Observatory (NSO) provide a consistent set of synoptic maps of the photospheric magnetic field between 1995 and 2003 which *Owens et al.* [2008] used in their analysis. However, these maps are unavailable for the time period of the Helios observations so WSA using NSO maps cannot be run for this exact period. It is important to use magnetograms from the same observatory for calibration and validation since discrepancies between observatories (e.g., processing, polar field fits, resolution, etc.) can lead to different coronal hole boundaries and hence use slightly different velocity equations. However, Figure 1a gives us confidence that the solar wind speed distributions observed during successive solar minima are very similar. So we used the WSA model results for the 41 Carrington rotations (years 1995–1997) used to produce Figure 2 to generate the model solar wind velocity distributions shown in Figure 5.

[20] Since the goal is to compare model velocity distributions with observations made in the ecliptic (i.e., within 7° of the solar equator) we use only the six model cells within 7.5° of the heliographic equator to create model velocity distributions. Nevertheless, from 41 Carrington rotations this provides over 35,000 individual velocity predictions.

[21] Figure 5a shows the normalized WSA velocity distribution obtained using the original velocity relationship, as used by *Owens et al.* [2008] but without the ad hoc modification described earlier (subtracting 50 km/s and limiting the range of speeds). This distribution is quite different from any of those in Figure 1. It has a single peak at 400 km/s and has no hint of the secondary peak evident in all the directly observed speed distributions. This distribution shows that WSA velocity relationship can be improved.

4.2. Fitting Velocity Distributions

[22] The four parameters in the velocity relationship we left adjustable are V_o, V_1, ϕ, and β. V_o governs the minimum

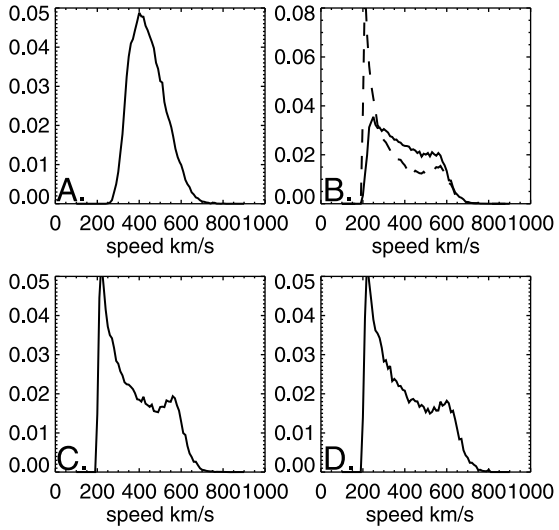

Figure 5. Normalized solar wind speed distributions from WSA using (a) the original empirical relationship used by *Owens et al.* [2008]: (b) $\phi = 3.6°$ (solid line) and $\phi = 4.1°$ (dashed line); (c) $\phi = 3.8°$ and $\beta = 3.6$; (d) $\phi = 3.8°$, $\beta = 3.6$, and $V_1 = 750$ km/s.

possible velocity. *Arge et al.* [2004] used $V_o = 240$ km/s, the minimum speed typically seen at 1 AU. However, Helios observed velocities as low as 200 km/s, so we lower V_o to 200 km/s. This value also agrees with *Schwadron and McComas* [2003] theoretical lower limit for the solar wind speed.

[23] In the velocity relationship the angle ϕ normalizes the angular distance of the foot of the flux tube from the nearest open flux boundary, θ_b. The general shape of the distribution is very sensitive to the value of ϕ. The two velocity distributions in Figure 5b were obtained using values of $\phi = 3.6°$ (solid line) and $\phi = 4.1°$ (dotted line) which highlights the sensitivity to ϕ. For large ϕ the distribution becomes sharply peaked at slow solar wind speeds. For small ϕ, the distribution widens, looking more like a broad square wave, becoming more gaussian as ϕ decreases even further. We find that values of ϕ between 3.6° and 4.1° (dependent on the values of other parameters in the velocity relationship) generate double peaked distributions similar to those observed.

[24] The value of β controls the distance to outer edge of the open flux boundary layer, represented by the vertical line in Figure 3. *Riley et al.* [2003] found that most of the slow solar wind originates from within 0.1 $R_\odot$, or about 6° from the edge of the open flux region (Figure 4). In order to choose optimal values of both ϕ and β we calculated the velocity relationship using six values of ϕ ranging from 3.6° to 4.1° and values of a between 2.6 and 4.1. For each value of ϕ we found the value of β which caused the outer edge of the boundary layer be closest to ~6°, indicated by the vertical line in Figure 3. We calculated the velocity distributions for each of these six pairs of ϕ and β and chose the one which compared best with the Helios observations (Figure 1b). The closest match was obtained using $\phi = 3.8°$ and $\beta = 3.6$, shown in Figure 5c.

[25] The last parameter in the empirical relationship to be adjusted, V_1, controls the maximum solar wind speed. *Schwadron et al.* [2005] showed that intermediate speed wind (600–740 km/s) comes from a boundary layer about 4° wide on the photosphere beyond the region of slow solar wind. The two vertical lines in Figure 2, drawn at $\theta_b = 6°$ and 10°, separate *Riley et al.*'s [2003] region of slow wind, Schwadron et al.'s region of intermediate speed wind, and the region of fast wind from well within the open flux regions. In the range of θ_b between the two lines (~6° < θ_b < ~10°) in Figure 2, the expansion factor, f_s, can have values of order 20 or larger. Such values of f_s never occur at larger values of θ_b. We adjusted V_1 so that the larger values of f_s that occur in this outer boundary layer produce intermediate speed wind. In particular we chose V_1 so that the solar wind speed for $f_s = 15$ and asymptotically large θ_b is 600 km/s (horizontal line in Figure 3). This required $V_1 = 750$ km/s.

[26] Figure 5d is the velocity distribution produced by our optimum set of velocity relation parameters: $V_o = 200$ km/s, $V_1 = 750$ km/s, $\phi = 3.8°$, and $\beta = 3.6$. This distribution should be compared with the Helios perihelion velocity distribution in Figure 1b. The match is not perfect, but it is a significant improvement over the velocity distribution given by the original velocity relationship shown in Figure 5a.

5. Evaluating the New Velocity Relation

[27] Since there are no in situ solar wind observations from the region near the Sun where we intend to make use of the velocity relation, we use the ENLIL solar wind model to propagate the WSA derived velocities out into the heliosphere. We then can compare the ENLIL solar wind predictions with observations made farther from the Sun. In order to test the velocity relation at both high and low heliographic latitudes we compared ENLIL predictions with observations from both Ulysses and near Earth.

5.1. Comparisons to Ulysses Fast Latitude Scan

[28] Figure 6 shows the solar wind speed measured by Ulysses during its first fast latitude scan in late 1994 and early 1995. The lower black line is the absolute value of the heliographic latitude of Ulysses (right-hand scale) which

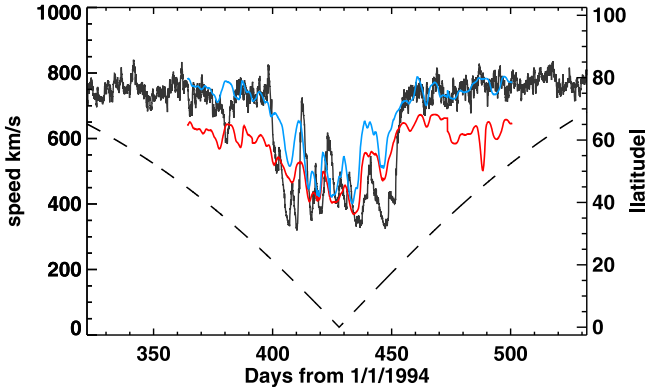

Figure 6. Ulysses solar wind speed observations during the 1994–1995 fast latitude scan (black) compared to the model solar wind speed predictions using the original (red) and new (blue) velocity relationships. The lower black line shows Ulysses' unsigned heliographic latitude (right axis). Time is measured in days from 1 January 1994.

went from poleward of 60° south to over 60° north during the time covered by Figure 6, crossing the equator close to the center of the plot. The upper, noisy black line shows the solar wind speed observed by Ulysses at a distance between 1.4 and 1.5 AU from the Sun. The sharp transitions from fast wind at higher latitudes to slow highly variable wind speed at lower latitudes occur on days 400 and 453 at latitudes of about 20° south and north respectively. The colored lines show the solar wind speed at Ulysses predicted by the WSA-ENLIL model using the original (red) and modified (blue) velocity relationships, respectively, for the 5 month period when Ulysses was below 50° latitude. This latitude range was chosen to minimize the edge effects from the ±60° latitude boundary of ENLIL. Using the original velocity relationship (red) WSA-ENLIL predicts too low a speed at high latitudes and fails to predict the large sharp variations in speed at low latitudes. The modified velocity relationship (blue) more accurately captures the fast speed polar wind and the large variations in speed near the equator. Thus the new velocity relationship reproduces the Ulysses observations far better than the original one.

5.2. Comparisons to 1 AU Observations

[29] *Owens et al.* [2008] compared solar wind speed predictions of several models, including WSA-ENLIL, with observations for the years 1995–2002. By comparing the mean, standard deviation and mean square error between the predicted and observed solar wind speed, *Owens et al.* [2008] showed that a new calibration of the WSA velocity equation was required. Following Owens et al., Figure 7 compares the solar wind speed observed by Wind (1995–1997) and ACE (1998–2003) with solar wind speed predictions from WSA-ENLIL using the original WSA velocity relationship (red) and the modified WSA velocity relationship (blue). Most of the highest observed solar wind speeds, especially in the solar maximum period 1999–2003, are due to passage of Interplanetary Coronal Mass Ejections (ICMEs) which are not included in the WSA-ENLIL model. Although the WSA-ENLIL model does not contain transients, it remains important to model the background solar wind conditions [*Case et al.*, 2008; *Owens*, 2008]. However, despite the presence of ICMEs, both the red and blue curves reproduce many of the recurring high-speed streams. However, the original velocity relationship (red) predicts a smaller variation in solar wind speed than is observed. This is especially clear during 1997 when the red trace fails to predict the slowest speeds observed. Qualitatively the modified WSA velocity relationship appears to match the observed solar wind speed better, especially during solar minimum.

[30] Quantitative comparisons are provided in Table 1 which lists the mean and standard deviation of the three time series and the root mean square (RMS) error between the two model predictions and the observations, as was done by *Owens et al.* [2008]. Using the original velocity relationship the average solar wind speed predicted over the 9 years is very close to the observed value, while the new velocity relationship predicts an average speed about 30 km/s larger. However, the standard deviation of the new velocity relationship predictions (103 km/s) is much closer to the observed value (99 km/s) which explains why the new velocity relationship predictions qualitatively match the observations in Figure 7 better than the original velocity relationship, despite having a higher RMS error. The greater variability in the new velocity relationship predictions results in a higher RMS error because of errors in the arrival times of streams [*Owens et al.*, 2005].

[31] The increase in the average solar wind speed using the new velocity relationship is mainly due to the increase in the maximum speeds of the predicted fast solar wind streams. The original velocity relationship tends to over predict slow solar wind speeds and under predict fast solar wind speeds during solar minimum. While during solar maximum, it under predicts both slow and fast solar wind speeds. This can be seen more clearly by comparing the distributions of solar wind speeds observed and predicted at 1 AU shown in Figure 8. The first two panels of Figure 8 show the normalized distributions of the observed solar wind speeds (black) and predicted solar wind speeds using the original velocity relationship (red) during solar minimum (1995–1997) and solar maximum (1998–2003), respectively. These distributions use larger bin sizes than in Figure 1, which smears out the bimodality of the distribution. For solar minimum the observed speed distribution peaks around 350 km/s. The original velocity relationship predictions peak closer to 450 km/s with a narrower and more symmetric distribution of speeds. As a result the old relationship over predicts slow solar wind speeds and under predicts the fast speed streams, predicting almost no speeds higher than 650 km/s, although the observations go up to 800 km/s. During solar maximum the two distributions are more similar and the peaks occur at the same speed, however the old relationship systematically under predicts the speed of both the fastest and slowest solar wind.

[32] The latter two panels of Figure 8 compare the distributions of the observed speeds (black) and the speeds predicted using the new velocity relationship (blue) during solar minimum and solar maximum. During solar minimum the new velocity relationship also over predicts the slow solar wind speeds but does a better job at capturing the speed of the fast solar wind streams. Again the model distribution peaks 100 km/s faster than observed distribution, but the width of the model and observed distributions are similar. The new velocity relationship predicts a greater proportion of both fast and slow wind, resulting in a broader distribution, which is much more consistent with observations. During solar maximum the new velocity relationship tends to slightly over predict the fast streams, leading to an average solar wind speed that is higher than the original model predicted. However, the observed and model speed distributions are very similar, both peaking at a little less than 400 km/s. The new WSA velocity relationship captures more high-speed streams, broadening the distribution and better matching observations.

[33] The new velocity relationship also predicts the arrival and speed of high-speed streams more accurately than the old relationship. To quantify this improvement we use the event-based analysis for high-speed enhancements (HSEs) in the solar wind developed by *Owens et al.* [2005]. They defined an HSE as a speed increase of at least 100 km/s within a period of 2 days. Using this criterion on the 9 years of solar wind observations 265 HSEs were found. Table 2 summarizes the observations/prediction comparison after pairs containing observational gaps within the 2 day time window were removed [*Owens et al.*, 2005]. Using the

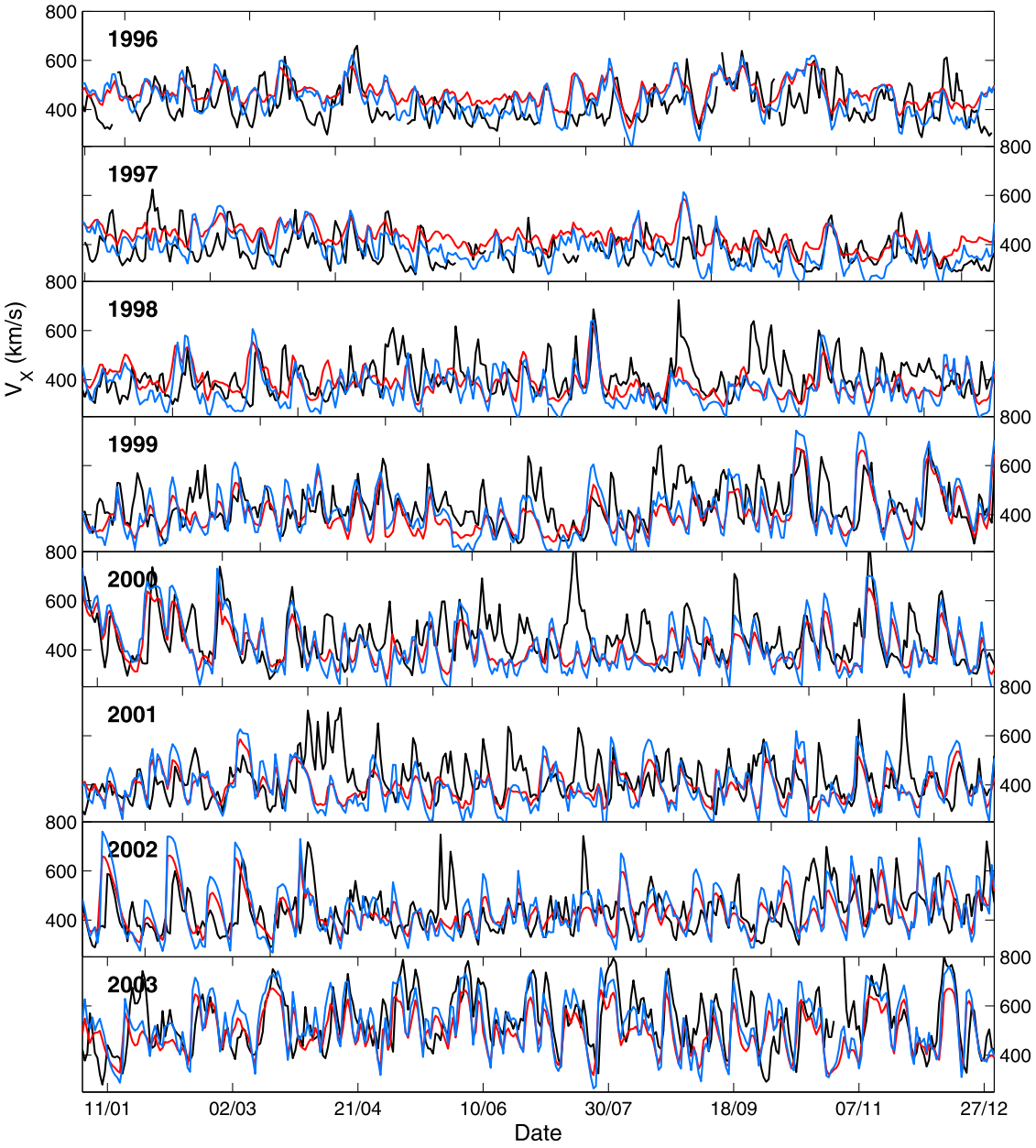

Figure 7. WSA-ENLIL solar wind speed predictions at Earth using the original (red) and new (blue) velocity relationships compared with observations (black) for the years 1996–2003. The comparisons are split into yearly rows, indicated by the bold year in the top left of each row, with the date (in month/day format) along the horizontal axis. The three curves have been smoothed to 24 h time resolution.

original velocity relationship, WSA-ENLIL predicted 128 HSEs; 107 of these were hits (that is, they occurred within 2 days of an observed HSEs), while 21 were false positives (that is, an HSE was predicted when none was observed). With the new velocity relationship, 193 HSEs were predicted, 155 hits and 38 false positives, about 50% more in both categories. Both relationships failed to predict a large number of observed HSEs (misses). This is not surprising since WSA-ENLIL is a steady state models that does not include ICMEs, which are present in the observations and often appear as HSEs in the analysis. The new velocity relationship, however, missed far fewer HSEs (102) than the original velocity relationship (148). The increased variability (larger standard deviation) for the new velocity relationship results in more speed enhancements meeting the criteria for

Table 1. Characteristics of the Observed and Modeled Solar Speeds for the Years 1995–2003

	Observed	WSA-ENLIL Original Equation	WSA-ENLIL New Equation
Mean V_x (km/s)	434	430	462
St. Dev V_x (km/s)	99	74	103
Root MSE (km/s)	-	97	115

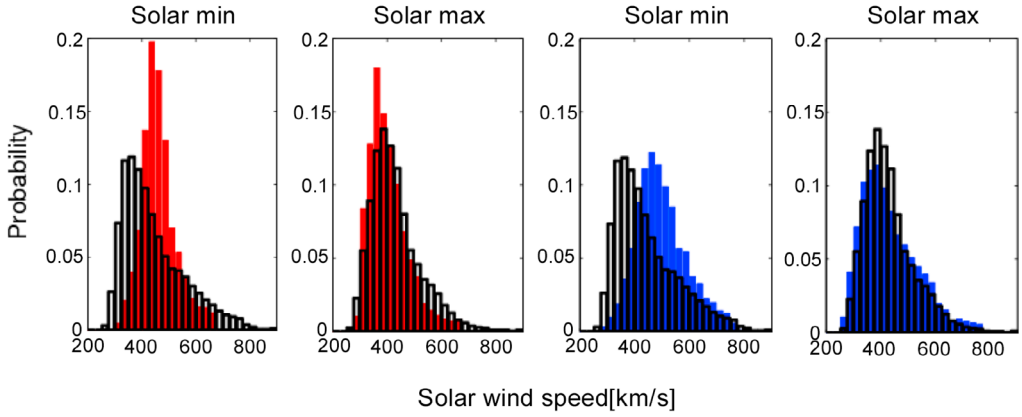

Figure 8. Observed solar wind speed distributions at 1.0 AU (black) compared with WSA-ENLIL predictions at 1.0 AU for solar minimum and solar maximum using the original WSA velocity relationship (red) and new velocity relationship (blue).

an HSE, especially during the solar minimum years 1995 and 1996.

[34] Both the number of accurately predicted HSEs (hits) and the number of false positives increased with the new velocity relationship. We use the "threat score" (also known as the Critical Success Index [*Schaeffer*, 1990]) to provide a statistical measure of the new velocity relationship's ability to predict events. The threat score provides a measure of prediction accuracy when true negatives are not important, as in this situation. The threat score is defined by equation (3), where NH, NM and NF are the number of hits, misses and false positives, respectively. Threat score values range from 1 (perfect) to 0.

$$TS = \frac{N_H}{N_H + N_M + N_F} \tag{3}$$

[35] The WSA-ENLIL threat score increases from 0.39 using the original velocity relationship to 0.53 using the new relationship. This increase quantifies our qualitative conclusion that the time series obtained using the new velocity relationship tracks the solar wind observations better, even though the root mean square error is larger. This analysis shows that the new velocity relationship not only predicts more HSEs, but that it also predicts them more accurately.

[36] *Owens et al.*'s [2008] analysis of HSEs in the WSA-ENLIL model also showed that the values of temperature and magnetic field components obtained from ENLIL were low compared with 1.0 AU observations. Since WSA-ENLIL uses the WSA solar wind speed to initialize number density, temperature and magnetic field strength on the inner boundary of ENLIL (0.1 AU), in the future the scaling of these other parameters will need to be studied and better tuned for use with the new solar wind velocity relationship. For example, the magnetic field strength at the inner boundary of ENLIL is calculated from the solar wind speed, so the increase in solar wind speeds at higher latitudes increases the initial magnetic field value in the inner heliosphere. This causes slightly higher solar wind speeds in the equatorial region at the fast/slow wind interface as ENLIL relaxes into a stable configuration. A better calibration of the magnetic field on the inner boundary would result in lower initial magnetic fields at higher latitudes, lower speeds in the equatorial region and a sharper transition between the fast and slow wind. This suggests that either a new calibration or a different computational algorithm that does not need such a calibration is required.

6. Sources of the Slow and Fast Solar Wind

[37] Figure 2 showed how nonuniformly the $\theta_b f_s$ plane is populated by values obtained from the WSA potential field model while in Figure 3 we examined the functional form of the velocity relationship showing how the solar wind speed varies as a function of θ_b and f_s. This empirical formula was calibrated independent of the distribution of θ_b and f_s seen in Figure 2 and we have yet to examine which parts of the curves in Figure 3 are populated by pairs of θ_b and f_s, obtained from the WSA potential field model. This is done in Figure 9 which combines the information in Figures 2 and 3. The new velocity relationship is plotted as contours of constant speed in increments of 50 km/s over the distribution of pairs of values of θ_b and f_s, obtained from the WSA model that were shown in Figure 2. As discussed earlier, the distribution of values of θ_b and f_s is far from uniform. Large values of f_s, (e.g., $f_s > 20$), only occur close to the open flux boundary ($\theta_b < 7°$). The velocity relationship contours fall into two distinct slopes, those that are almost vertical and those that are nearly horizontal. Slow speed wind ($V_{SW} <$

Table 2. Contingency Tables Showing the Number of Hits, Misses, and False HSEs Using the WSA-ENLIL Model With the Original and New Solar Wind Velocity Relationships

	Observations	
	HSE	No HSE
HSE[a]	107	21
No HSE[a]	148	-
HSE[b]	155	38
No HSE[b]	102	-

[a]WSA-ENLIL: original equation.
[b]WSA-ENLIL: new equation.

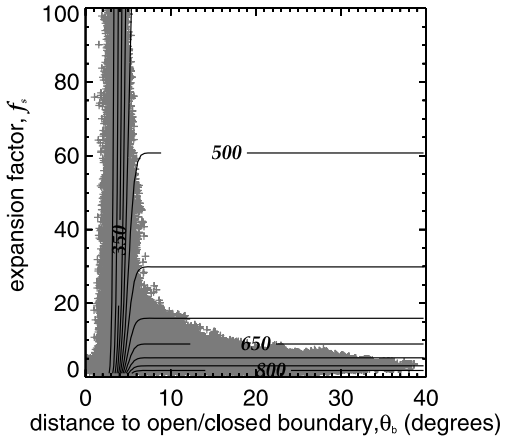

Figure 9. Scatterplot of expansion factor versus distance from the open flux boundary distance of open flux tubes seen in the WSA model for 41 Carrington rotations (1890–1930) during solar minimum from Figure 2 overlaid with contours of the velocities predicted by WSA using the new velocity relationship.

500 km/s) all comes from within 6° of a open flux boundary and the speed is controlled primarily by the distance to that boundary, as only the vertical parts of these contours overlay the shaded region of the plot. On the other hand, solar wind faster than 600 km/s comes exclusively from beyond this boundary region and is controlled primarily by the expansion factor (horizontal contours). There only is a narrow transition region around $\theta_b \approx 6°$ where the curved contours, indicating a dependence on both the expansion factor and open flux boundary distance, overlay the shaded region.

[38] Figure 9 shows us that the model, during solar minimum, gives two distinct types of solar wind, whose speed is controlled by different factors. The slow wind arises from close to the open flux boundary and its speed depends almost entirely on the distance from the flux boundary and not on the expansion factor. Conversely the fast solar wind arises from well into the open flux region and its speed is completely determined by the expansion factor. The resulting speed variation of about 150 km/s is qualitatively consistent with the range of fast solar wind speeds seen by Ulysses when deep within the polar open flux regions. Figure 6 (between days 450 and 500) shows how well the expansion factor variations can reproduce the fluctuations in solar wind speed observed within the polar coronal hole.

[39] Although one can imagine other possible mechanisms to control the distance from the open flux boundary and expansion factor dependence for the slow and fast wind, we believe the simplest explanation is that the speeds of the fast and slow solar winds are controlled by different factors. This strongly suggests that the fast and slow solar winds have distinct acceleration mechanisms and that the bimodal speed distribution in both Figures 1 and 5d really is the result of combining two separate solar wind populations.

7. Summary and Conclusions

[40] We have recalibrated the WSA velocity relationship for the solar wind velocities in the inner heliosphere (0.1 AU). Once recalibrated the velocity relationship was used as the inner boundary condition for ENLIL, a heliospheric MHD model. This recalibration results in a velocity distribution which better matches Helios observations made near perihelion and, when propagated out into the heliosphere with the ENLIL model, leads to improved solar wind predictions at both 1AU and Ulysses. Although the new velocity relationship was obtained using only solar minimum data, we extended the validation to include solar maximum. When compared with observations made near Earth over a 9 year period, the speeds derived using the new velocity relationship had a larger mean square error than those derived from the original relationship. However, the solar wind speed variability, the number of HSEs predicted, and the threat score all improved. Furthermore, the comparison with Ulysses observations showed a dramatic improvement in the match with solar wind speeds at higher latitudes. These results provide confidence that the new velocity relationship improves predictions of the solar wind speed not only near Earth, but also throughout the ENLIL solution domain in the inner heliosphere beyond the 0.1 AU inner boundary and at all latitudes.

[41] The bimodal distribution of the Helios velocity observations made closer to the corona suggest two separate populations of solar wind speeds, a fast wind and a slow wind. The empirical velocity relationship in we obtained (Figure 9) shows that fast solar wind arises far from the open flux boundary with a speed primarily determined by the expansion of the field, while the slow solar wind arises from within about 6° of the open flux boundary, with a speed determined by that distance and with very little dependence on expansion factor. The range of expansion factors that occurs within the slow solar wind region is large, exceeding 100. These expansion factors are much larger than those invoked to control solar wind heating and compositional variations [*Cranmer et al.*, 2007; *Wang et al.*, 2009] which were less than 20 for their solar minimum solution. However, the expansion factors found within the fast solar wind region are smaller(less then 20) and so these ideas could apply there.

[42] The dependence of the WSA slow solar wind speed on the distance from the open flux boundary is consistent with interchange reconnection of loops at coronal hole boundaries being the source of the slow solar wind. In reality this region is probably composed of both open and closed field lines, but the potential field model relaxes to a minimum energy state, making this region entirely open. Although these sources would be inherently dynamic, statistically the slower solar wind would arise from interchange reconnection with loops in the corona that the model suggests have a source closer to the open/close flux region boundary.

[43] The recalibration of the WSA velocity relationship strongly suggests that the solar wind in the corona during solar minimum consists of two separate populations. The speeds of these two populations (slow and fast) are controlled by different parameters, the distance from the open flux boundary and the expansion factor, consistent with two separate theories of the solar wind acceleration, interchange reconnection of coronal loops and the magnetic field expansion factor, respectively. Perhaps a combination of these ideas is necessary to explain the solar wind speed in the outer corona.

[44] **Acknowledgments.** This work was supported by the Center for Integrated Space Weather Modeling, which is funded by the STC program of the National Science Foundation under Cooperative Agreement ATM-0120950. The OMNI data were obtained from the Goddard Space Flight Center(GSFC)-SPDF OMNIWeb interface at http://omniweb.gsfc.nasa.gov. The authors would also like to acknowledge H. Rosenbauer (PI) and R. Schwenn for Helios 1 plasma data, NSSDC, and GSFC-SPDF.

[45] Philippa Browning thanks Marcia Neugebauer and another reviewer for their assistance in evaluating this paper.

References

Altschuler, M. A., and G. Newkirk (1969), Magnetic fields and the structure of the solar corona, *Sol. Phys.*, *9*, 131–149.

Arge, C. N., and V. J. Pizzo (2000), Improvement in the prediction of solar wind conditions using near–real time solar magnetic field updates, *J. Geophys. Res.*, *105*, 10,465–10,479.

Arge, C. N., D. Odstrcil, V. J. Pizzo, and L. R. Mayer (2003), Improved method for specifying solar wind speed near the Sun, in *Solar Wind Ten*, *AIP Conf. Proc.*, vol. 679, edited by M. Velli, R. Bruno, and F. Malara, pp. 190–193, Am. Inst. of Phys., New York.

Arge, C. N., J. G. Luhmann, D. Odstrcil, C. J. Schrijver, and Y. Li (2004), Stream structure and coronal sources of the solar wind during May 12th, 1997 CME, *J. Atmos. Sol. Terr. Phys.*, *66*, 1295–1309.

Banaszkiewicz, M., W. Axford, and J. McKenzie (1998), An analytic solar magnetic field model, *Astron. Astrophys.*, *337*, 940–944.

Case, A., H. Spence, M. Owens, P. Riley, and D. Odstrcil (2008), Ambient solar wind's effect on ICME transit times, *Geophys. Res. Lett.*, *35*, L15105, doi:10.1029/2008GL034493.

Cranmer, S. (2005), Why is the fast solar wind fast and the slow solar wind slow? A survey of geometrical models, in *Solar Wind 11/SOHO-16: Connecting the Sun and Heliosphere*, edited by B. Fleck, T. Zurbuchen, and H. Lacoste, pp. 159–164, Eur. Space Agency, Noordwijk, Netherlands.

Cranmer, S., A. A. van Ballogooijen, and R. Edgar (2007), Self-consistent coronal heating and solar wind acceleration from anisotropic magnetohydrodynamic turbulence, *Astrophys. J. Suppl. Ser.*, *171*, 520–551.

de Toma, G., and C. N. Arge (2005), Multi-wavelength observations of coronal holes, in *Large-Scale Structures and Their Role in Solar Activity: Proceedings of the 22nd Sacramento Peak Workshop, Held at the National Solar Observatory, Sacramento Peak, Sunspot, New Mexico, USA, 18–22 October 2004*, vol. 346, edited by K. Sankarasubramanian et al., pp. 251–260, Astron. Soc. of the Pac., San Francisco, Calif.

de Toma, G., C. N. Arge, and P. Riley (2005), Observed and modeled coronal holes, in *Connecting Sun and Heliosphere: Proceedings of Solar Wind 11/SOHO 16: 12–17 June 2005, Whistler, Canada*, pp. 609–612, Eur. Space Agency, Noordwijk, Netherlands.

Fisk, L. A., and N. A. Schwadron (2001), Behavior of the magnetic field of the Sun, *Astrophys. J.*, *560*, 425–438.

Fisk, L. A., N. A. Schwadron, and T. H. Zurbuchen (1998), On the slow solar wind, *Space Sci. Rev.*, *86*, 51–60.

Fisk, L., G. Gloeckler, T. Zurbuchen, J. Geiss, and N. Schwadron (2003), Acceleration of the solar wind as a result of the reconnection of open magnetic flux with coronal loops, in *Solar Wind Ten*, *AIP Conf. Proc.*, vol. 679, edited by M. Velli, R. Bruno, and F. Malara, pp. 287–292, Am. Inst. of Phys., New York.

Gosling, J., J. Asbridge, S. Bame, and W. Feldman (1978), Solar wind stream interfaces, *J. Geophys. Res.*, *83*, 1401–1412.

Leer, E., and T. Holzer (1980), Energy addition in the solar wind, *J. Geophys. Res.*, *85*, 4681–4688.

McGregor, S., W. Hughes, C. Arge, and M. Owens (2008), Analysis of the magnetic field discontinuity at the potential field source surface and Schatten Current Sheet interface in the Wang-Sheeley-Arge model, *J. Geophys. Res.*, *113*, A08112, doi:10.1029/2007JA012330.

Odstrcil, D. (2003), Modeling 3-D solar wind structure, *Adv. Space Res.*, *32*, 497–506.

Owens, M. J. (2008), Combining remote and in situ observations of coronal mass ejections to better constrain magnetic cloud reconstruction, *J. Geophys. Res.*, *113*, A12102, doi:10.1029/2008JA013589.

Owens, M. J., C. N. Arge, H. E. Spence, and A. Pembroke (2005), An event-based approach to validating solar wind speed predictions: High-speed enhancements in the Wang-Sheeley-Arge model, *J. Geophys. Res.*, *110*, A12105, doi:10.1029/2005JA011343.

Owens, M. J., H. E. Spence, S. L. McGregor, W. J. Hughes, C. N. Arge, P. Riley, J. A. Linker, and D. Odstrcil (2008), Metrics for solar wind prediction models: Comparison of empirical, hybrid and physics-based schemes with 8 years of L1 observations, *Space Weather*, *6*, S08001, doi:10.1029/2007SW000380.

Pneuman, G. (1980), The physical structure of coronal holes—Influence of magnetic fields and coronal heating, *Astron. Astrophys.*, *81*, 161–166.

Riley, P., J. A. Linker, and Z. Mikic (2001), An empirically-driven global MHD model of the solar corona and inner heliosphere, *J. Geophys. Res.*, *106*, 15,889–15,901.

Riley, P., Z. Mikic, J. A. Linker, and T. H. Zurbuchen (2003), Understanding the solar sources of in situ observations, in *Solar Wind Ten*, *AIP Conf. Proc.*, vol. 679, edited by M. Velli, R. Bruno, and F. Malara, pp. 79–82, Am. Inst. of Phys., New York.

Schaeffer, J. T. (1990), The critical success index as an indicator of warning skill, *Weather Forecasting*, *5*, 570–575.

Schatten, K. H. (1971), Current sheet magnetic model for the solar corona, *Cosmic Electrodynamics*, *2*, 232–245.

Schatten, K. H., J. M. Wilcox, and N. F. Ness (1969), A model of interplanetary and coronal magnetic fields, *Sol. Phys.*, *6*, 442–455.

Schwadron, N. A., and D. J. McComas (2003), Solar wind scaling law, *Astrophys. J.*, *599*, 1395–1403.

Schwadron, N. A., D. J. McComas, H. A. Elliot, G. Gloeckler, J. Geiss, and R. Von Steiger (2005), Solar wind from the coronal hole boundaries, *J. Geophys. Res.*, *110*, A04104, doi:10.1029/2004JA010896.

Wang, Y. M., and N. R. Sheeley (1990), Solar wind speed and coronal flux-tube expansion, *Astrophys. J.*, *355*, 726–732.

Wang, Y. M., and N. R. Sheeley (1992), On potential field models of the solar corona, *Astrophys. J.*, *392*, 310–319.

Wang, Y. M., Y. K. Ko, and R. Grappin (2009), Slow solar wind from open regions with strong low coronal heating, *Astrophys. J.*, *691*, 760–769.

C. N. Arge, Kirtland Air Force Base, Bldg. 464, Rm. 403, 3550 Aberdeen Ave. SE, Albuquerque, NM 87117, USA.

W. J. Hughes and S. L. McGregor, Astronomy Department, Boston University, 725 Commonwealth Ave., Boston, MA 02215, USA. (slmic@bu.edu)

D. Odstrcil, NASA Goddard Space Flight Center, Mail Code 674, Greenbelt, MD 20771, USA.

M. J. Owens, Department of Meteorology, University of Reading, Earley Gate, Reading RG6 6BB, UK.